Materials Science and Engineering A 527 (2010) 5637–5647

Contents lists available at ScienceDirect

Materials Science and Engineering A

journal homepage: www.elsevier.com/locate/msea

Adhesion at Al-hydroxide-polymer interfaces: Influence of chemistry and evidence for microscopic self-pinning

W.P. Vellinga[a,b,*], G. Eising[b], F.M. de Wit[a,c], J.M.C Mol[a,c], H. Terryn[a,d], J.H.W. de Wit[a,c], J.Th.M. De Hosson[a,b]

[a] Materials Innovation Institute, M2i, Mekelweg 2, 2628 CD, Delft, The Netherlands
[b] Materials Science, Applied Physics, University of Groningen, Nijenborgh 4, 9747 AG, Groningen, The Netherlands
[c] Materials Science and Engineering, 3Me, Delft University of Technology, Mekelweg 2, 2628 CD Delft, The Netherlands
[d] Electrochemistry and Material Science, Department of Metallurgy, Vrije Universiteit Brussel, Pleinlaan 2, 1050 Brussels, Belgium

ARTICLE INFO

Article history:
Received 19 January 2010
Received in revised form 7 May 2010
Accepted 10 May 2010

Keywords:
Adhesion
Aluminium hydroxide
Pseudo-boehmite
Delamination
Crack pinning

ABSTRACT

We present a combined chemical (auger electron spectroscopy) and microscopic (optical microscopy, scanning electron microscopy and scanning probe microscopy) study of the work of adhesion and delamination mechanisms at interfaces between a glassy polymer (glycol-modified polyethylene terephthalate) and Al covered with different types of surface hydroxides. A clear correlation between the measured work of adhesion and the chemical nature of the Al surface, specifically the hydroxyl coverage and the iso-electric point is found. The magnitude of the work of adhesion points to important contributions from plastic deformation in the glassy polymer for some cases. Delamination is shown to be accompanied by the formation of microscopic shear bands at such interfaces. The non-monotonous stress–strain behaviour of the glassy polymer that gives rise to the shear bands is also shown to lead to peculiar pinning events at the crack front. Evidence indicates that the occurrence of protrusions in the crack front deriving for example from the presence of stress concentrators and crack initiation sites ahead of the front, combined with mode and rate dependence of the local energy release rate along the front may pin the front at positions adjacent to a protrusion. It is believed such microscopic mode-dependent pinning phenomena may be relevant for the adhesion on patterned interfaces.

© 2010 Elsevier B.V. All rights reserved.

1. Introduction

The adhesion of organic coatings on aluminium is an important industrial topic for example in the packaging of food and beverages. The native oxide on aluminium is stable only in neutral environments (pH 4–8) where no chlorides are present. In the case of aluminium alloys precipitates form cathodic or anodic sites where localized corrosion can initiate. One way of protecting aluminium alloys from corrosion is by using an organic polymeric coating and for effective protection it is essential that such coatings adhere well to the alloy substrate. The general aim of the work presented here is to increase the understanding of de-adhesion at interfaces between a glassy polymer and oxide- or hydroxide-covered metals. To accomplish the aim both the correlation between interface chemistry and work of adhesion, and between work of adhesion and delamination mechanisms is studied in detail. The specific interfaces that are treated exist between glycol-modified polyethylene terephthalate (PETG) and oxy-hydroxide layers on pure and low alloyed Al (Al (99.999%) and AA1050) and an Al–Mg alloy, AA5182. This paper studies the influence that acidic, alkaline and boiling water pre-treatments have on these interfaces. It presents data on surface chemistry and bonding to a model compound and formulates a hypothesis on the expected bonding to PETG. It then extends those studies by determining the interface chemistry and work of adhesion of such interfaces and by studying the associated microscopic de-adhesion mechanisms in microscopic detail using *in situ* techniques. The materials and surface treatments used may be relevant for industrial practice, however the adhesion treatment and the thickness of the PETG layer were optimised for the experimental work carried out here.

In delamination or de-adhesion along interfaces between glassy polymers and metals different types of bonds interact. The metallic bonds are (in general) much stronger than the interchain van der Waals interaction in the glassy polymer, as can be judged from their respective moduli that typically differ by 2 orders of magnitude.

The bonding across the interface itself depends on the chemistry of both metal and polymer. Which types of bonds exist across the interface is not clear *a priori* because in general oxide or hydroxide

* Corresponding author at: Materials Science, Applied Physics, University of Groningen, Nijenborgh 4, 9747 AG, Groningen, The Netherlands.
Tel.: +31 503634821; fax: +31 503634881.
E-mail address: w.p.vellinga@rug.nl (W.P. Vellinga).

0921-5093/$ – see front matter © 2010 Elsevier B.V. All rights reserved.
doi:10.1016/j.msea.2010.05.020

Table 1
Hydroxyl coverage (OH) and effective surface area(A/A_0) determined by XPS and BET. From ref. [22].

AA1050	Alkaline	Acid	H_2O
OH	43	35	47
A/A_0	1.6	1.4	15

layers cover a metal surface and both their chemical and physical nature depend on the pre-treatment of the metal surface.

For an atomically flat interface the bond chemistry and density at the surface is important in determining the measured energy release rate. The interaction between polymers and metals is thought to be due to relatively weak hydrogen bonds the strength of which depends on the chemical nature of the interface. Assuming 10 hydrogen bonds per nm^2 and 4–100 kJ/mol [1] as bounds on the bonding energy this would lead to a energy release rate G of 1.7 J/m^2 at maximum, which is a rather low value. Such low values will only be measured if the interface bonds are very weak compared to those in the surrounding materials and both bond stiffness and maximum bond strength are relevant. But importantly the stiffness and strength of H-bonds can be of the same magnitude as those of the secondary bonds within a glassy polymer. This means that if a H-bond "connected" to a glassy polymer is loaded it may lead to substantial (visco-)elastic or potentially plastic deformation in the glassy polymer.

The chemical character of the native oxide layer on Al and Al alloys can be influenced by surface treatments and a distinction between acidic, alkaline and boiling water surface treatments is useful. Of particular relevance here are studies that deal with the bonding of the ester functional groups (C(=O)O) that occur in PETG. For AA1050 the influence of pre-treatments on the bonding of ester-based model compounds was studied by van den Brand et al. [22]. The carbonyl groups in the ester are positively charged and form so-called Lewis acids. The groups are able to accept electrons from electron donors. Hydroxyl groups present on the aluminium surface are able to donate electrons through the negatively charged O, and thus act as a Lewis base. Hydrogen bonds may be formed between the acid and base. van den Brand et al. [22] were able to determine the chemical nature of the bonds as well as the area fraction of the surface covered in –OH groups. Their results are shown in Table 1.

Using XPS measurements they found minor differences in the chemical behaviour of the aluminium cations for surface oxides after acid and alkaline pre-treatment. It was shown that the hydroxyl fraction is significantly higher after alkaline pre-treatment than after acid pre-treatment. Acid and alkaline pre-treated substrates showed an increase of effective surface area A/A_0 with a factor of 1.4 and 1.6 as shown by BET techniques [22].

In case of AA5182 differences in surface chemistry come into play. The strength of the hydrogen bonds is positively correlated with the difference in iso-electric point (IEP) between the bonding species, which offers a way of qualitatively establishing interface bond strengths in these cases [14]. The IEP of a surface (that can be measured with colloid titration) is defined as the pH at which it has no net electrical charge. A low IEP indicates an acidic surface and a high IEP indicates an alkaline surface. The values of the IEP are 12 for magnesium oxide (MgO) and 8 for aluminium oxide (Al_2O_3), respectively [15]. Using inverse gas chromatography it has been determined that PETG is a weak base [10]. It is therefore expected that the hydrogen bond between MgO and PETG is stronger than between Al_2O_3 and PETG.

On the surface of AA5182 oxides of both Mg and Al may be expected and considering their different IEP a surface treatment that influences the relative surface coverage of these oxides may also be expected to influence the adhesion to ester containing polymers. Di-methylterephthalate (DMT) as a probe is expected to be especially relevant. With DMT as a probe on AA5182 it was found that alkaline and boiling water pre-treatment lead to a bonding interaction whereas acid pre-treatment does not. Similar findings were obtained for AA1050 [3].

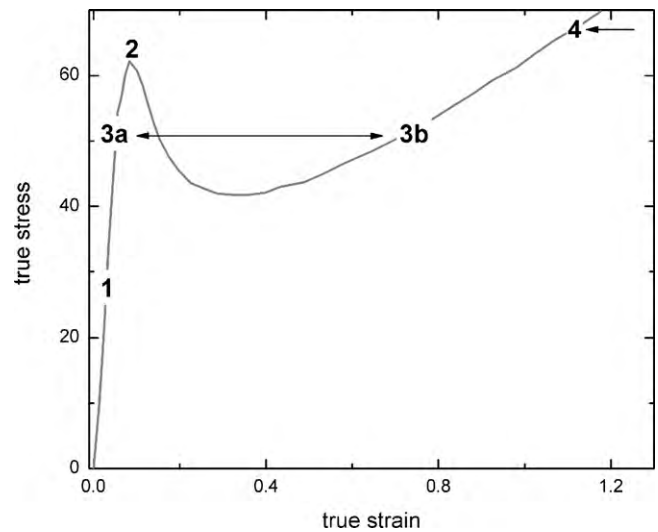

Fig. 1. True stress in MPa vs. true strain for PETG (after [5]). Numbers are used in the text to discuss the properties of PETG and again in Fig. 7 to discuss microscopic delamination mechanisms.

The pre-treatment with boiling water cannot be easily compared to the other two since it dramatically changes the interface geometry. Using BET techniques van den Brand concluded that the effective surface area of AA1050 increased by a factor of 14.6 after a boiling water treatment [22] associated with the formation of a nano-structured pseudo-boehmite oxi-hydroxide layer (see Fig. 4). Such pseudo-boehmite layers are known to be particularly effective in increasing adhesion between metals and polymers such as PET and PE [19]. Rider reported [18] a boiling water pre-treatment to an aluminium substrate and effects on adhesion and the durability of an applied epoxy coating. Strålin and Hjertberg [20] found that an ethylene vinyl acetate polymer has a stronger bonding with a pseudo-boehmite aluminium hydroxide layer than with a dehydroxylated aluminium oxide.

The effects of substrate surface roughness on the adhesion of polymer coatings were extensively studied by [4,13,12,16,9,26,6]. It was found that adhesion at a rougher surface can indeed lead to an increased energy release rate. Often, dissipative mechanisms are triggered near the interface in the bulk of the metal and the polymer. By concentrating stress in the polymer at tips of fibers or along ridges of flakes for example, local plastic deformation may be induced that adds to the total work of adhesion. For glassy polymers this is an especially relevant issue because the (macroscopic) stress–strain curve of these materials generally shows initial softening behaviour after a yield stress before hardening occurs (see Fig. 1).

The peculiar shape of the stress–strain curve means that after the yield stress (point 2 in Fig. 1) is reached the material can deform spontaneously to a much higher strain level while at the same time reducing the local stress (e.g. points 3a and 3b in Fig. 1). Energy is then dissipated in the polymer by the formation of shear bands and no large scale de-adhesion needs to take place. If the ultimate stress in the polymer (e.g. point 4 in Fig. 1) is higher than that of the interface de-adhesion may take place along the polymer-oxide interface, or possibly through the oxide layer or along the Al-oxide interface. Dissipation in the polymer is known to be important in determining the work of adhesion since measured values are often

much higher than the values expected from breaking all available bonds at the interface.

Finally it should be noted that the interfaces may also be chemically heterogeneous. In the case of the Al alloys for example precipitates exist at or near the surface. These precipitates do not cover a large fraction of the surface but they may differ in adhesion properties.

2. Experiment

2.1. Materials

2.1.1. Aluminium

For the main experiments three types of Al were used: Al (99.999%), AA1050 (99.5 wt% Al) and AA5182, an aluminium–magnesium alloy (4.8 wt% Mg). The samples were ground and polished with a final polishing step of 0.25 μm. They were then cleaned in acetone and hot chloroform (99+ vol.% pure), left to dry and subjected to further pre-treatments as described below. The substrates used had dimensions of 60 mm × 10 mm × 1.5 mm. For all alloys a Young's modulus of 70 GPa, a Poisson's ratio of 0.33 and a thermal expansion coefficient of $23.8 \times 10^{-6}\,K^{-1}$ were used in the calculations.

Polished substrates where subjected to 3 different pre-treatments to obtain different kinds of hydrous oxide layers [2]. For the acid pre-treatment aluminium substrates were immersed in a 30 vol.% HNO_3 solution in deionised water for 30 s. After 30 s the substrates were rinsed using deionised water for at least 1 min and blown dry using nitrogen gas.

For the alkaline pre-treatment sodium hydroxide grains (98 vol.% pure) were dissolved in deionised water until a solution with pH 12.5 was obtained, as measured by a calibrated pH meter. The aluminium substrates were placed in the solution for 30 s. Finally the substrates were rinsed using deionised water for at least 60 s and blown dry using nitrogen gas.

For the third pre-treatment the substrates were placed in boiling water for 60 s, resulting in a pseudo-boehmite (AlOOH) layer [24]. After immersion the substrates were blown dry with nitrogen gas and allowed to cool down for 3 min.

To determine the influence of the immersion time for the HNO_3 (see below) pre-treatment an AA2024 alloy covered with a layer of commercially pure Al was used. Samples measured 65 mm × 10 mm × 1 mm. The substrates were not polished in order to keep the pure Al layer intact. To remove dirt they were cleaned using deionised water, methanol and acetone. The samples were dried using a spin-coater. To reduce bending of the samples during measurements a piece of AA5182 with equal dimensions was glued to the sample, increasing the overall thickness to 2.5 mm.

2.1.2. PETG

Glycol-modified polyethylene terephthalate (PETG) was used as polymer coating in the experiments. This polymer is a form of polyethylene terephthalate (PET) and is created by (partly) replacing ethylene glycol in the polymer backbone by cyclohexane dimethanol. This lowers the melting temperature of the polymer creating a polymer more suitable, for e.g. thermoforming. PETG remains essentially amorphous independent of the temperature treatment that it receives. This in contrast with semi-crystalline PET. The PETG coatings were 300 μm thick. The films were obtained from Bayer and cut to pieces of 70 mm × 6 mm. The pieces were cleaned in an ultrasound bath in subsequent steps using soap, ethanol and deionised water. After cleaning they were put between two ultrasonically cleaned glass plates and left to dry for at least 48 h at 50 °C. The material properties used are Young's modulus of 2 GPa, a Poisson's ratio of 0.40 and a thermal expansion coefficient of $55 \times 10^{-6}\,K^{-1}$.

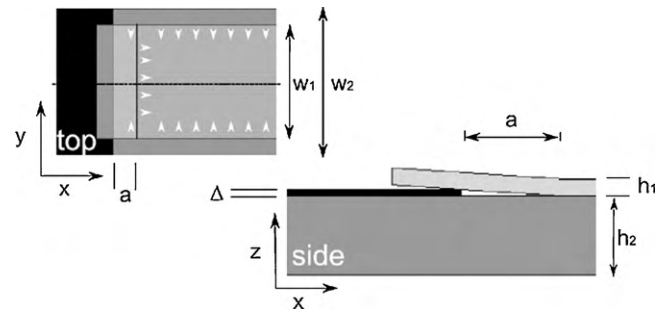

Fig. 2. Sketch of experimental set-up with relevant geometrical parameters.

2.1.3. ADCB samples

Samples for the ADCB setup were made by placing a PETG strip between a pre-treated aluminium substrate and a cleaned glass plate coated with 3M Novec(tm) Electronic Coating EGC-1700. This coating was applied to prevent adhesion between the glass plate and the PETG strip. Steel plates were positioned at both sides of the sample to improve heat conduction. To exert a constant pressure, springs are clamped around the stack. The spring-loaded stack is placed in a pre-heated aluminium holder in the oven for 3 min at 150 °C. The samples are then left to cool down to room temperature for at least 30 min.

2.2. Techniques

2.2.1. Surface chemistry

AES measurements were performed using a PHI 650 scanning Auger microprobe system with an energy resolution Δ of 0.5% for Al compounds. The beam current was set to 20 μm and the primary electron beam to 5 keV. The scan area of the electron beam was approximately 130 μm by 130 μm. Depth profiling was done using an argon ion beam with a gun voltage of 3.5 kV and a gun current of 10 μA to obtain a sputtering rate of 4 nm/min for Al_2O_3. The sputtered area was 3 mm by 3 mm. From measured AES spectra the chemical composition was determined using principal component analysis (PCA). Component spectra from external standards were compared with the component spectra found by PCA in a target factor analysis (TFA) [27].

Samples analyzed were sputter-cleaned for 20 s beforehand to remove possible dirt. To further eliminate the influences of possible contaminants the high energy KL_2L_2 Auger lines were used to interpret the Auger spectra. For aluminium and aluminium oxide these lines are at 1396 eV and 1378 eV, respectively. For magnesium and magnesium oxide the KL_2L_2 Auger lines are at 1186 eV and 1174 eV. Compensating for the sensitivity factor for aluminium and magnesium the element concentrations were calculated.

2.2.2. Energy release rate

To determine the adhesion energy and crack propagation the asymmetric double cantilever beam (ADCB) method was used, schematically depicted in Fig. 2. In the ADCB method, a parallel sided knife is inserted in a pre-crack initiated at the interface between the metal and polymer. The moment exerted by the blade leads to the propagation of the crack front to a certain equilibrium position at which point the decrease in stored elastic energy equals the increase in interface energy.

Usually the blade is moved at a constant speed, and a dynamically stable situation sets in with the crack front propagating at the applied velocity with a velocity dependent crack length. Using the thickness of the blade, the crack length and the elastic material

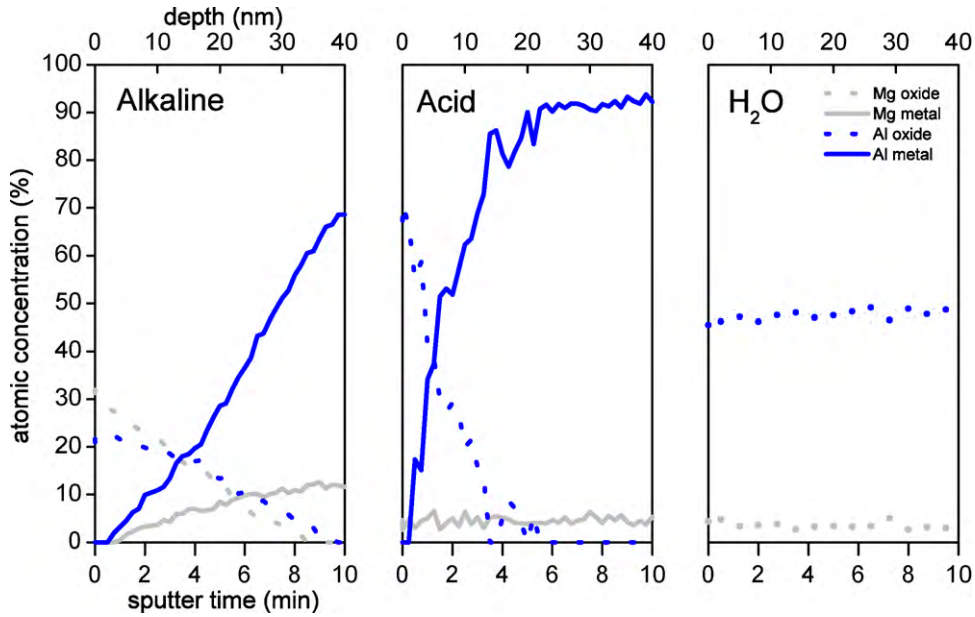

Fig. 3. Depth profiles obtained from AES measurements on polished aluminium AA5182 after applying different pre-treatments. Carbon (atomic concentration ¡5% and Oxygen were also included in the TFA but are not shown for clarity.

properties one can calculate the energy release rate G associated with delamination along the interface.

Relevant parameters of the experimental set-up are sketched in Fig. 2. To force substrate and coating apart work per unit area equalling the effective work of adhesion, or the energy release rate G has to be performed. In ADCB two driving forces for debonding may be present: the mechanical load caused by the knife or wedge and the thermal residual stresses. The energy per unit area associated with thermal mismatch and processing is defined as G_T (the "thermal" energy release rate) and the mechanical energy per unit area as G_M (the "mechanical" energy release rate). The total energy release rate G can be found by adding these terms provided that the materials behave as a linear elastic continuum and that the deflections of the beams are small [8]:

$$G = G_M + G_T \tag{1}$$

For G_M Kanninen [11] derived:

$$G_M = \frac{3\Delta^2 E_1 h_1^3 E_2 h_2^3}{8a^4}\left[\frac{E_1 h_1^3 C_2^2 + E_2 h_2^3 C_1^2}{(E_1 h_1^3 C_2^3 + E_2 h_2^3 C_1^3)^2}\right] \tag{2}$$

with $C_1 = 1 + 0.64h_1/a$ and $C_2 = 1 + 0.64h_2/a$. (It should be noted that this expression for G_M is used even when a very small volume of the material near the interface deforms plastically as will be shown later. This is justified by the fact that these deformations are not expected to change the effective bulk elastic modulus of the PETG layer significantly. Therefore the elastic energy stored in the PETG beam is still given by 2.)

For G_T we take

$$G_T = \frac{1-\nu^2}{E_c}\sigma_0^2 h_c \tag{3}$$

with

$$\sigma_0 = \frac{E_c \Delta\alpha \Delta T}{1-\nu_c} \tag{4}$$

representing the equi-biaxial residual thermal stress. (Near the edges the residual stress is relaxed in the direction perpendicular to the edge. This results in a somewhat reduced value for G_T. This effect is small for $h_c << w_1$ and is neglected in the following.)

ADCB experiments were performed in a reflection optical microscope with a circular polariser and a digital camera connected to a computer for data acquisition. The transparency of the PETG layer allows microscopic real-time *in situ* study of the delamination processes that are taking place [30,28]. (Typical delamination fronts of ADCB experiments for the three pre-treatments are shown in Fig. 5.) All measurements were performed using a knife speed of 15 μm/s unless mentioned otherwise. The energy release rate was determined by measuring the thickness of the aluminium substrate (h_1) and the PETG coating (h_2) and the crack length a, defined as the distance between the knife contact line and the center of the crack front. For each averaged value shown in Table 2 at least 3 samples were used, with at least 15 measurements per sample. The errors were determined by calculating the standard deviation of all measurements for a given pre-treatment on a given alloy.

3. Results

3.1. Surface composition after pre-treatment

To determine the composition of the hydrous oxide layer after a pre-treatment on the AA5182 alloys AES depth profiling measurements were performed as described in Section 2.2.1. For the AA5182 alloy the near-surface composition was expected to consist of magnesium and aluminium, both metallic and oxidised. TFA was applied using spectra of both metals and oxides. The resulting depth profiles are shown in Fig. 3.

For the AA1050 alloy no AES depth profiling was performed as the samples have a low fraction (< 0.005) of Mg. (Using scanning electron microscopy-energy X-ray dispersive spectroscopy (SEM-EDS) no Mg was found in the top layer of the pre-treated AA1050 substrates.)

The depth profile obtained for acid pre-treated AA5182, see Fig. 3, shows that the Mg concentration at the surface is low, slightly lower than the bulk value. This can be explained by the corrosiveness of the acid solution for the Mg. Mg will react with the solution at the surface and be slightly depleted.

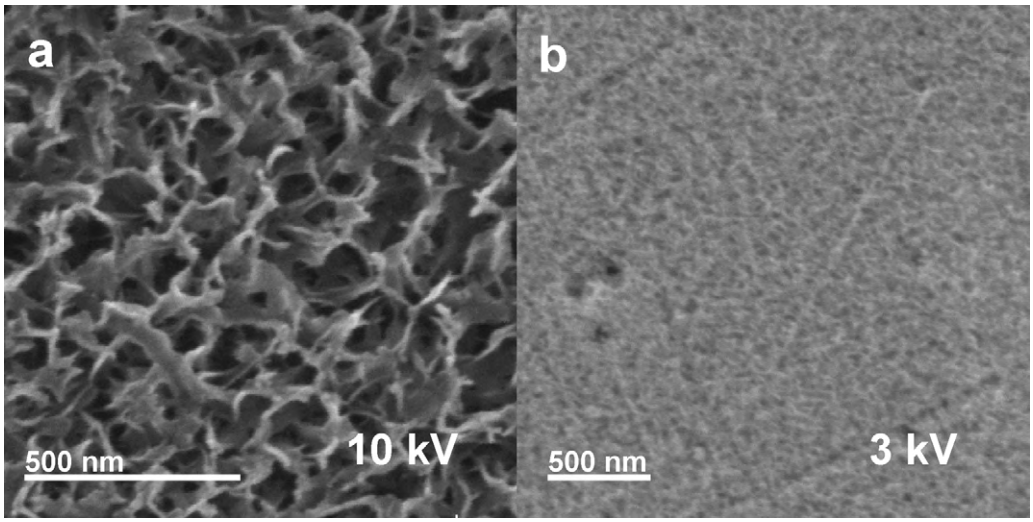

Fig. 4. (a) The pseudo-boehmite layer formed on polished AA5182 after 60 s in boiling water. (b) Nano-structured hydroxide of Mg and Al formed on a polished AA5182 after 60 s alkaline pre-treatment.

The depth profile after the alkaline pre-treatment (Fig. 3) indicates a high concentration of Mg oxide at the surface, slightly higher than the concentration of Al oxide. This is due to the fact that $Mg(OH)_2$ is stable only above pH 12 where Al (hydr-)oxides are not [17].

The near-surface depth profile of boiling water pre-treated AA5182 is shown in Fig. 3. At the surface only a very low Mg oxide fraction is measured. As Mg oxide is hygroscopic and will dissolve in the water it attracts, this is in fact expected.

From the AES depth profiles an indication of the oxide layer thickness can be obtained. The thickness is defined here by the depth at which the oxide concentration is equal to the Al metal concentration. Using the sputter rate and time (see Section 2.2.1), the thickness of the layer removed is determined. For the acid pre-treatment the layer has a thickness of 3 nm. For the alkaline pre-treatment a thickness of 23 nm is determined. For the boiling water pre-treatment the layer thickness is found to be > 40 nm. The thickness of the oxide layers after alkaline and boiling water pre-treatment is much higher than that of native oxides and therefore the surface structure must have been drastically altered.

SEM images of the resulting surface structures are shown in Fig. 4.

On immersing polished AA1050 and AA5182 substrates in boiling water a nano-porous layer is quickly formed at the surface, as can be seen in Fig. 4. This layer is known from the literature to be an amorphous pseudo-boehmite structure with the composition $Al_2O_3 \cdot H_2O$ [25,21]. It turns out that the alkaline-treated AA5182 shows a somewhat similar microstructure but much less pronounced, see Fig. 4b. Based on the AES measurements this is thought to be a mixed oxide/hydroxide of Mg and Al.

3.2. Energy release rates

Energy release rates as determined from the ADCB experiments are shown in Table 2.

Table 2
Energy release rates for different pre-treatments, obtained from ADCB measurements.

Pre-treatment	AA1050 (J/m^2)	AA5182 (J/m^2)
Acid	10 ± 2	8 ± 2
Alkaline	21 ± 3	30 ± 3
Boiling water	79 ± 15	73 ± 13

For both alloys the samples pre-treated with boiling water show the highest energy release rates, and the acid pre-treated samples show the lowest energy release rates. It can also be observed that values of G after acid and boiling water pre-treatments are equal for AA1050 and AA5182. The alkaline pre-treated samples show lower energy release rates for AA1050 than for AA5182. The alkaline pre-treated AA5182 shows better adhesion than acid pre-treated AA5182.

For both alloys $G_{boil} > G_{Alk} > G_{Ac}$ and it is found that $G_{Alk}^{1050} < G_{Alk}^{5182}$. Furthermore, $G_{boil}^{1050} \approx G_{boil}^{5182}$ and $G_{Ac}^{1050} \approx G_{Ac}^{5182}$. In a qualitative sense these results are entirely reasonable based on our earlier discussion of the importance of surface chemistry and specific area.

We recall that the geometry of three of the surfaces was drastically altered by the pre-treatments and start to discuss relations between the surfaces of which the changes were predominantly chemical.

The fact that $G_{Alk}^{1050} > G_{Ac}^{1050}$ is attributed to the increased density of hydroxyl groups on the surface as was shown in XPS measurements [23].

On the other hand the fact that $G_{Alk}^{1050} > G_{Ac}^{1050}$ is attributed to the increased presence of magnesium oxide on the surface of the AA5182 sample as found by the AES depth profiling. Since MgO has a higher IEP value than Al_2O_3, it is effectively raising the IEP value of the oxide layer. Due to the larger difference in IEP value between the oxide and the PETG coating stronger hydrogen bonds are expected to form [1], improving the adhesion. G_{Ac}^{1050} and G_{Ac}^{5182} are comparable, which is reasonable because the surface of AA5182 is depleted of Mg after acid treatment and the chemistry of both surfaces has become rather similar.

Now we turn to results involving the boiled samples and the alkaline-treated AA5182.

The fact that $G_{Alk}^{5182} > G_{Ac}^{5182}$ cannot solely be attributed to a chemical cause, but the increased presence of Mg oxides combined with the increased specific surface are both in accordance with that.

For the boiled surfaces covered with pseudo-boehmites we find that G_{boil}^{1050} does not differ significantly from G_{boil}^{5182}. The AES measurements on AA5182 indicate that there is very little Mg oxide in the pseudo-boehmite layer, so presumably the chemistry of the pseudo-boehmite layers on AA1050 and AA5182 do not differ too much. Judging from the SEM images their geometry is also similar. Together this explains the fact that the energy release rates turn out to be equal.

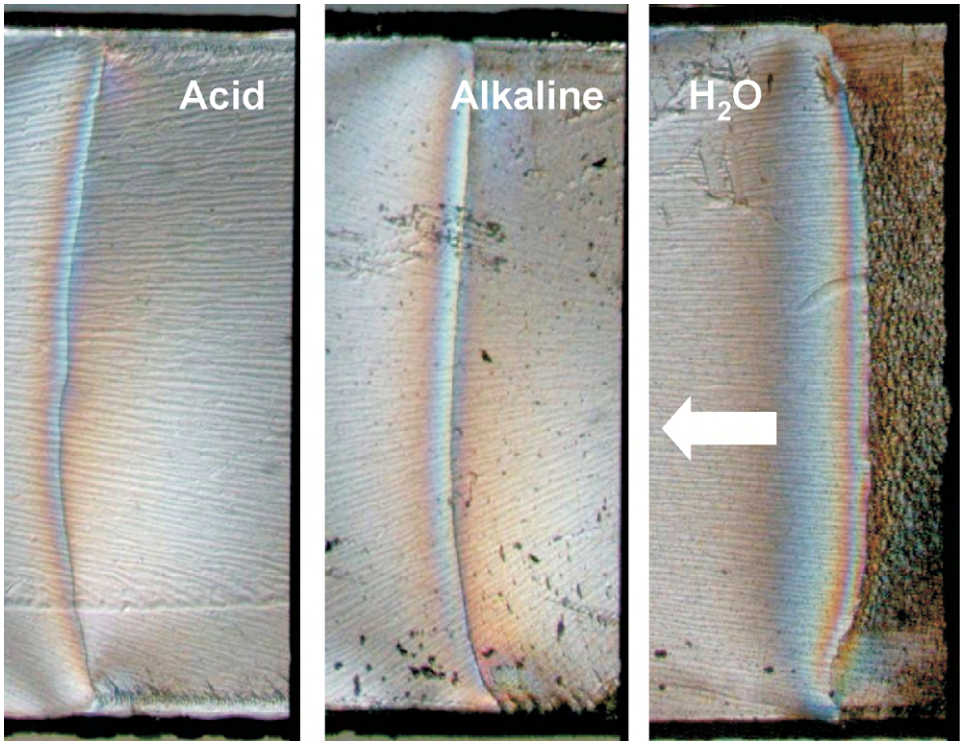

Fig. 5. Images taken during ADCB measurements for different pre-treatments. The inserted knife blade is visible as the dark field to the right. It should be noted that this is not the contact point with the crack faces used in the determination of the crack length since the otherwise flat knife ends in a wedge. The crack fronts are positioned directly to the right of the fringes. The arrow indicates the direction of front movement for all three cases.

Comparing the boiled samples with all others it is clear that they have by far the largest energy release rate. We conclude that the high specific surface caused by the nano-structured pseudo-boehmite dominates in these cases.

This concludes the discussion of the qualitative correlation of chemistry, specific surface and energy release rate. So far we have ignored the discussion of the quantitative values. In fact those values indicate that plastic deformation in the poly-

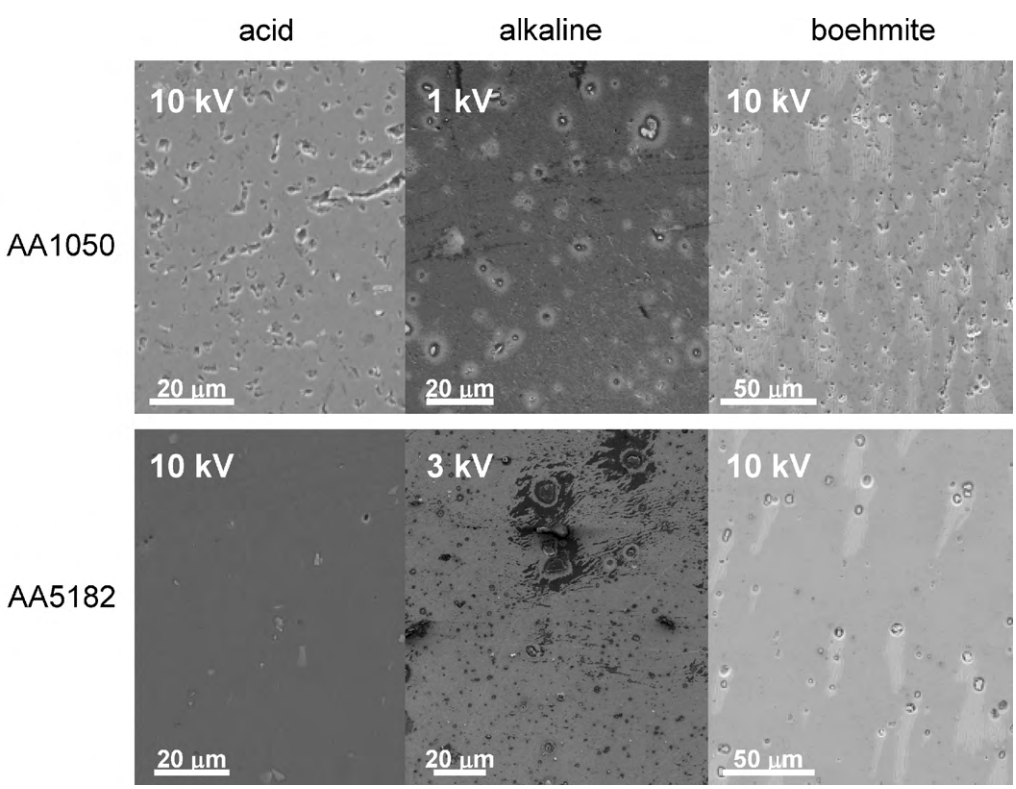

Fig. 6. SEM micrographs of the Al side of the delamination plane.

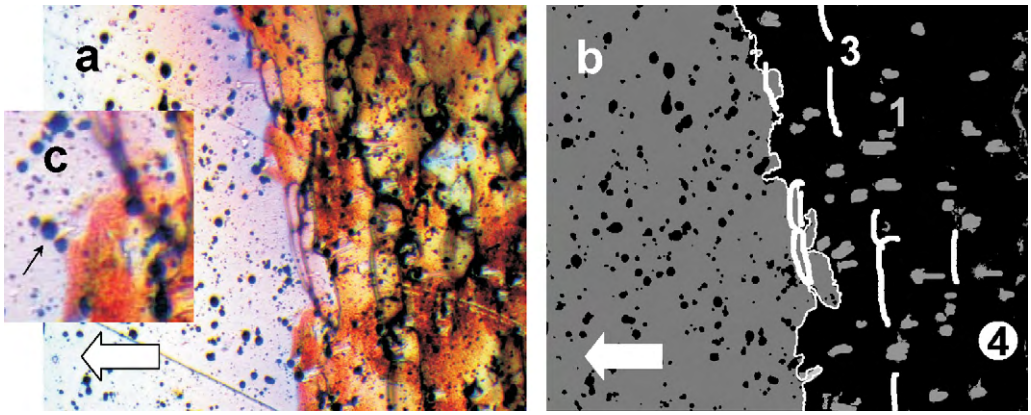

Fig. 7. (a) Progressing front along a boehmite–PETG interface. The detail behind the crack front visible in Fig. 5 is identified as the thin and thick black lines. (b) Sketch of the same showing crack front (thin white line), precipitates on the crack plane ahead of front (dark patches to the left), shear bands extending into the PETG (thick white lines), "comets" on the crack plane behind the front (gray patches to the right). Numbers match the gray level of the phenomenon they indicate and correspond to the numbers in Fig. 1. (c) A detail of (a) that shows that the "comets" form ahead of the crack front.

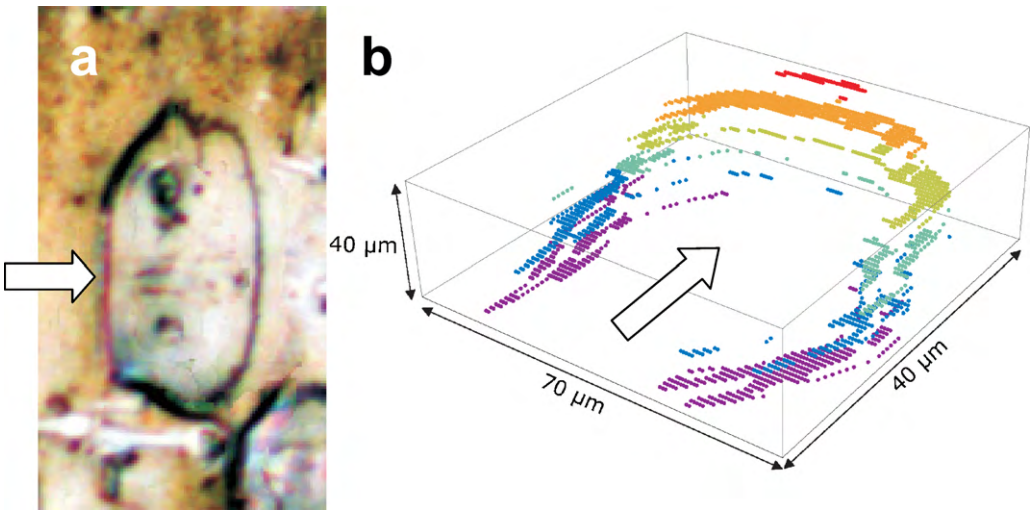

Fig. 8. (a) A single in-focus image derived from a stack of images of a typical shear band found in the PETG coating and (b) 3D reconstruction of the same.

mer plays a role in delamination, and quite substantially so in case of the pseudo-boehmite covered surfaces. Both real-time *in situ* optical and post-mortem microscopy of various types indicate that is indeed the case, and this evidence will be discussed next.

3.3. Microscopy

Optical images representative of the moving crack fronts are shown in Fig. 5 and representative SEM images of the Al surfaces after delamination are shown in Fig. 6. These serve as starting points for our discussion.

Comparing the optical micrographs in Fig. 5 reveals a large difference in optical reflectivity behind the crack front between the alkaline and acid-treated samples on the one hand, and the boiled samples on the other hand.

Whereas the samples with acid and alkaline pre-treatment are almost featureless in that region at this scale, the sample with the boiling water pre-treatment shows very prominent microstructural features. Also the crack front in that case is much rougher.

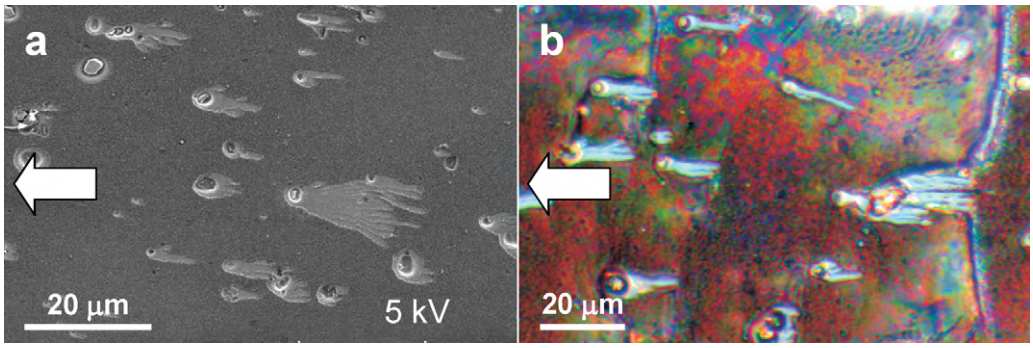

Fig. 9. "Comet" like features formed during delamination on both faces of boiled (pseudo-boehmite covered) AA1050–PETG interface crack. (a) AA1050 side. (b) PETG side.

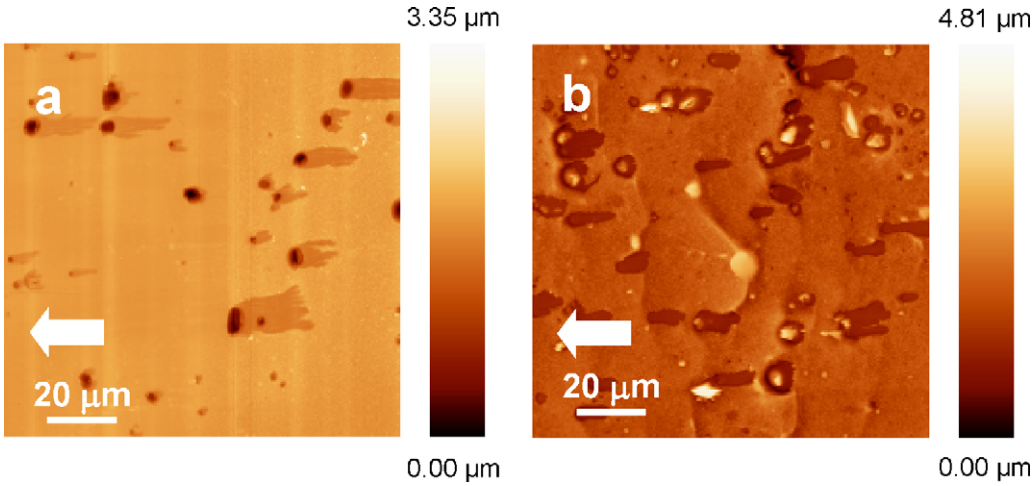

Fig. 10. AFM images of "comets" formed during delamination on the Al (a) and PETG (b) side of a boiled (pseudo-boehmite covered) AA1050–PETG interface. Note that the "comets" are depressions on both crack faces.

On acid-treated AA1050 and AA5182 and alkaline-treated AA1050, at low acceleration voltages (e.g. 1 kV) a difference in SE yield occurs between delaminated (lower SE yield) and not delaminated areas (higher SE yield) (not shown). This would suggest that some carbon remains at the delaminated surface. However it does not occur in a form that leads to a clearly discernible microstructure.

The situation is quite different in the alkaline-treated AA5182 and the samples treated with boiling water where the surface structure after pre-treatment shows the presence of nano-structured hydroxides. From the SEM images (Fig. 6) of the delamination planes it is clear that the presence of these oxides has the potential of drastically altering the delamination mechanisms. On the boiled samples there is a profusion of "comet"-like features, of which the "head" is centered on a precipitate and the "tail" stretches from the "head" in the direction opposed to the crack front movement. On the alkaline-treated AA5182 the situation is slightly more complex. It is concluded that in most parts the hydroxide layer has delaminated, however it remains in isolated locations, and surrounds all larger precipitates. Isolated chunks of PETG are observed as well.

The task is now to reconcile the SEM (post-mortem) and optical (*in situ* and real-time) observations on the boiled samples.

3.4. Delamination mechanisms on interfaces with pseudo-boehmite

Fig. 7 shows an image of part of a crack front. Many details are visible in the figure some of which are indicated in Fig. 7b.

3.4.1. Shear bands

The features in common with Fig. 5 are identified as the rough thick and smooth thin black lines visible behind and at the crack front. The nature of these lines becomes clearer from a 3D analysis of the crack plane on the PETG side after delamination. By moving the focal plane through the PETG layer using steps of 2 μm a Z-stack of images is obtained. On each image a Sobel edge detection algorithm is used to isolate the black lines. Noise is reduced by first applying a simple threshold and subsequently a closing filter. Subsequently a single 3D image combining only in-focus information of all images in the stack is created. Coding the set of images for the height at which they were obtained and recombining them height-maps or 3D reconstructions can be obtained. A typical result is depicted in Fig. 8.

It is determined that the thin black lines trace out a curved plane in the polymer interpreted here as a plane of localized shear deformation. These shear bands have a depth (in the direction of movement of the knife) of 40–200 μm, a width of 20–70 μm and a height of 20–50 μm.

The rough thick black lines are seen to be associated with the part of the shear band nearest its base on the crack plane and the smooth thin black lines with the part of the shear band extending out into the bulk of the polymer away from the approaching crack front.

Fig. 7 also helps to clarify the relation of these shear bands to the crack front. It turns out that between the shear bands the crack has propagated slightly further, meaning that the localized shear bands act as *pinning centers* for the crack front. As the crack front propagates at some instant the locally pinned part of the front will catch up. Also visible in Fig. 7 is that the delamination of coating near the shear band happens by mode-III propagation from both sides of the shear band base.(Apart from this local pinning, pinning on the scale of the sample indicated by the crack front curvature is also observed. This is not discussed any further here, see for example [29] and references therein.)

3.4.2. Local delamination or "comets"

Fig. 9 shows micrographs of the Al and PETG side of the crack plane that show important similarities and differences. The main difference between the Al side and the PETG side is in the shear bands discussed in the previous section. Perpendicular to the propagation direction of the crack front we observe ridges of varying size which we identify as the "bases" of shear bands. The similarities are the "comet-like" features which Fig. 9 clearly shows on both sides of the interface.

From the observations we conclude that all "comets" consist of a precipitate or a void left by a precipitate at one side and a "tail" on the other side. Note that the "tails" are actually always on the side where the blade was inserted. Lengths are ranging from 1 μm to 50 μm.

Using AFM Fig. 10b was obtained which shows that the "tails" are depressions, or holes in the hydroxide layer. The maximum depth of the "comet tails" ranged between 200 nm and 300 nm. For similar hydroxide layers thicknesses of 200 nm have been reported [7]. That would mean that the whole hydroxide layer is locally removed from the aluminium substrate and that the polished surface is exposed. In accordance with that SEM-EDS showed a spectrum comparable to that of an untreated polished substrate. This indicates that locally the bonding of the hydroxide layer with the Al substrate may fail.

An AFM measurement on the PETG crack-face is shown in Fig. 10b. The shear band bases are now visible as ridges with

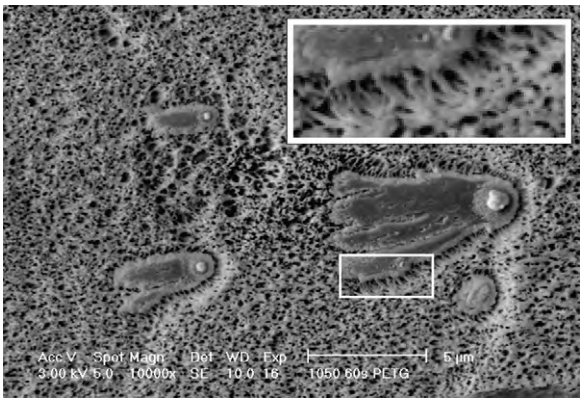

Fig. 11. Image SEM of the "comets" on the PETG side of a boiled AA1050–PETG interface. The enlarged inset illustrates the occurrence of crazing on the PETG side.

heights of up to 500 nm. Counter to intuition, the "comets" are again observed as depressions in the crack-face. The typical depth measured here was 2 μm.

Additional information is gained from a SEM image obtained of the PETG crack-face depicted in Fig. 11. Using SEM-EDS on a comet Al is found. This confirms the hypothesis that a part of the hydroxide layer stays locally attached to the PETG coating and is removed from the Al substrate during crack propagation. Clearly the presence of Al on the PETG side makes clear that the holes on this side are not due to the fact that part of the PETG is detached during the crack propagation.

In fact the AFM and SEM images of the PETG side contain clues why the "tails" show up as depressions on both sides. Both images show the effects of crazing on the PETG crack-face. This is perhaps most clear in the SEM images at edges of the "comets", see the inset in Fig. 11. In areas were the crack front propagated along the PETG-oxide interface, fibrils were created as shown in the inset in Fig. 11 which show a detail of the edge of a "comet". These fibrils are not formed were the crack front propagated through the oxide layer or along the oxide-Al interface meaning that lower stresses are acting on the area of the "comet tails". This can be explained as follows: a combination of stress concentration and locally weak bonding means that precipitates at the surface of the Al substrate are dislodged and locally delamination is initiated *ahead* of the crack front. Small cracks start to propagate from the precipitate through the hydroxide layer in the direction of the global crack front, i.e., forming the "tails" of the "comet". When the "tails" reach the crack front the crack front will locally advance. (An example of this phenomenon is not shown not shown for these interfaces but compare Fig. 12.)

3.4.3. *Evidence for microscopic "self-pinning"*

With the "comets" appearing ahead of the front (Fig. 7c) the possibility exists that they are somehow related to the appearance of the shear bands, and therefore to local pinning, at the crack front. Clearly the local loading mode is altered by the introduction of protrusions or sharp corners at the crack front. Moreover the local loading history is altered since points of the interface just ahead of the comet experience a rather different stress build-up than points some distance away. Considering that the mechanical behaviour of the PETG is time-dependent and that the energy release rate is mode-dependent, potentially these local differences may induce the formation of shear bands. This suggests that the small comet-like cracks might induce pinning points for the shear bands.

It was decided to check this with experiments at similar interfaces *without* the precipitates that appear to induce the local comet-like delaminations. This was attempted by repeating the experiments with Al 99.999%. Mechanical polishing of the ADCB samples proved impractical and instead electropolishing was used. A simple modification of an existing electropolishing machine produced an acceptable finish across the whole sample surface and crack plane. The samples were glued to AA5182 strips to provide rigidity during preparation.

A typical result is shown in Fig. 12. The optical micrograph in the figure clearly shows the crack front. A clear contrast is visible between the undelaminated, rather smooth, and delaminated part that shows "background" detail on a fine scale and a number of triangular shaped features.

Precipitates are absent at these interfaces and at the scale of the "comets" of the Al alloys crack propagation on these interfaces is much more uniform. This suggests that the presence of the precipitates and the crack propagation mode on the alloys are indeed linked. The small scale background detail is thought to be associated with plastic deformation of the PETG when it delaminates from the substrate.

The triangular features stand out precisely because they lack the small scale detail, and look much more like the undelaminated part. This suggests that the original interface structure is partly intact and that delamination through the pseudo-boehmite or along the pseudo-boehmite Al interface has taken place.

The triangular shape itself is reminiscent of the "comet tails" observed on the Al alloy interfaces, and its orientation with respect to the progressing crackfront is the same. Interestingly, near the "crack front corners" thin lines associated with shear deformation are observed, suggesting that the local mode change induced by the appearance of the triangular protrusion in the crack front is indeed effective in initiating shear bands. The shear bands introduced here are rather small and isolated and were not seen to be effective in pinning the front. However, the relation between local mode changes and the appearance of shear bands is clearly established by this observation.

Together these results on the Al5N support the counterintuitive hypothesis that the presence of weak spots on the interface may lead to a higher work of adhesion because they induce local changes in opening mode. These local changes in the loading of the crack front may locally pin the front by offering alternative stress release mechanisms, such as in this instance shear banding.

This leaves the only the structure at the crack plane of alkaline-treated AA5182 to be discussed. In some of the samples the hydroxide layer behaved much as the pseudo-boehmite layers, with local delamination of the hydroxide from the Al substrate. Using AFM a thickness of about 15 nm for the hydroxide layer was estimated (based on the depth of depressions found on the substrate surface) which is in reasonable agreement with the results presented in Table 2. In some cases the geometry of the delamination features was somewhat similar to that of boiled samples with triangular features with the same orientation. However the phenomenology was found to differ quite a bit between samples with different times of pre-treatment. Longer treatment times (60 s) lead to very homogeneous delamination planes. Carefully observing the samples at a glancing angle with the naked eye showed some colour contrast between delaminated and non-delaminated areas and this was also apparent in micrographs with 5 kV SE SEM. No signs of local delamination events of the hydroxide layer were apparent on such interfaces, and delamination is thought to occur through the hydroxide layer or along the PETG hydroxide interface. On the other hand shorter treatment times led to the more complex interface structures as shown in Fig. 6, that in essence show three different delamination paths: through the PETG, along the PETG hydroxide interface and along the Al-hydroxide interface. On such interfaces the hydroxide layer remains around precipitates suggesting that the chunks of PETG that are visible on some locations are connected to a precipitate. Evidently for these relatively thin hydroxide

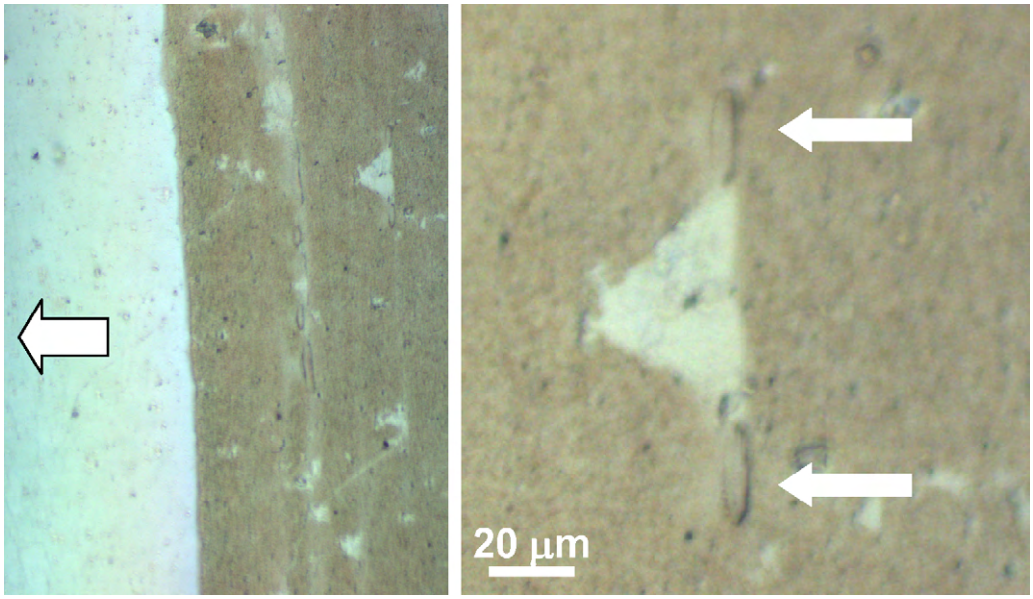

Fig. 12. Optical micrographs of local triangular delaminated areas near a Al5N–PETG interface. Local shear bands are associated with the two corners where the local crack coalesced with the main crack. These are presumed to be initiated by the different mode mixity at the corners.

films the effect of differing treatment times is larger than for the thick ones formed during boiling, and more work is needed in this regard. However, the results show that the delamination of these thin layers can be much like that of the thick layers on the boiled samples.

4. Conclusions

The work of adhesion between PETG and smooth acid and alkaline pre-treated Al surfaces can qualitatively be understood in terms of the difference in IEP between the polymer and the hydroxide layers formed by the pre-treatment.

A much higher work of adhesion is found for Al alloys pre-treated with boiled water and in this case the increase in specific surface area due to the formation of nano-structured pseudo-boehmite dominates the chemistry.

High interface stresses (higher than the yield stress of PETG) between PETG and Al alloys covered in nano-structured pseudo-boehmite combined with the occurrence of softening in the stress–strain behaviour of PETG leads to the appearance of localized shear bands near a propagating crack tip.

Shear bands near a crack tip typically measure tens of microns in directions along the front and into the PETG. These shear bands locally reduce the loads on the interface and propagating fronts are observed to be pinned locally by such local shear bands.

The chemical inhomogeneity caused by the presence of precipitates leads to locally differing adhesion. On the pseudo-boehmite covered substrates such differences lead to initiation of delamination around precipitates some distance ahead of the crack front. These locally initiated cracks then propagate towards the crack front delaminating a more or less triangular area.

Local delamination effects ahead of the crack front may lead to the formation of localised shear bands at the front, presumably because of the local difference in mode-mix introduced at the crack front.

The results support the counterintuitive hypothesis that the presence of weak spots on the interface may lead to a higher work of adhesion because of induced local changes in crack opening mode. These local changes in the loading of the crack front may locally pin the front by offering alternative stress release mechanisms, such as in this instance shear banding.

It is believed such mechanisms may be of importance in the development of patterned interfaces with engineered adhesion properties.

Acknowledgments

This work is part of the research programme of the Materials Innovation Institute, Delft, the Netherlands, and funded under grants MC7.05223 and MC6.04196

References

[1] J.C. Bolger, A.S. Michaels, Molecular Structure and Electrostatic Interaction At Polymer–Solid Interfaces, Plenum Press, New York, 1983.
[2] F.M. de Wit, J.M.C. Mol, H. Terryn, J.H.W. de Wit, Journal of Adhesion Science and Technology 22 (2008) 6017.
[3] F.M. De Wit, Ö. Özkanat, J.M.C. Mol, H. Terryn, J.H.W. De Wit, Surface and Interface Analysis 42 (4) (2010) 316–320.
[4] E. Detsi, Crack propagation in mixed-mode delamination at polymer–metal interfaces. Master's thesis, University of Groningen, 2008.
[5] B. Rebecca, C. Dupaix, Mary, Boyce, Polymer 46 (13) (2005) 4827–4838.
[6] A.V. Fedorov, R. van Tijum, W.P. Vellinga, J.Th.M. De Hosson, Progress in Organic Coatings 58 (February (2–3, Sp. Iss. SI)) (2007) 180–186.
[7] J.D. Gorman, A.E. Hughes, D. Jamieson, P.J.K. Paterson, Corrosion Science 45 (6) (2003) 1103–1124.
[8] S. Guo, D.A. Dillard, J.A. Nairn, Journal Of Adhesion 26 (2006) 285–294.
[9] A.F. Harris, A. Beevers, International Journal of Adhesion and Adhesives 19 (1999) 445.
[10] L. Jia, Y.P. Wang, B. Wang, M.J. He, Q.R. Zhang, B.L. Shi, Journal of Macromolecular Science Part B-Physics 47 (2008) 378.
[11] M.F. Kanninen, International Journal of Fracture 9 (1973) 83.
[12] M.P. Larsson, M.M. Ahmad, Journal of Micromechanics and Microengineering 16 (6) (2006) 161–S168.
[13] H.-Y. Lee, J. Qu, Journal of Adhesion Science and Technology 17 (2) (2003) 195–215.
[14] E. McCafferty, Journal of the Electrochemical Society 150 (2003) 342.
[15] E. McCafferty, J.P. Wightman, Journal of Colloid and Interface Science 194 (1997) 344–355.
[16] D.E. Packham, International Journal of Adhesion and Adhesives 23 (2003) 437.
[17] M. Pourbaix, Atlas of Electrochemical Equilibria in Aqueous Solutions, Pergamon Press, 1966, p. 1.
[18] A.N. Rider, Journal of Adhesion Science and Technology 15 (2001) 395–422.
[19] A. Strålin, T. Hjertberg, Journal of Adhesion Science and Technology 7 (1993) 1211.
[20] A. Strålin, T. Hjertberg, Journal of Applied Polymer Science 49 (3) (1993) 511–521.
[21] A. Strålin, T. Hjertberg, Applied Surface Science 74 (1994) 263.
[22] J. van den Brand, O. Blajiev, P.C.J. Beentjes, H. Terryn, J.H.W. de Wit, Langmuir 20 (15) (2004) 6318–6326.

[23] J. van den Brand, P.C. Snijders, W.G. Sloof, H. Terryn, J.H.W. de Wit, The Journal of Physical Chemistry B 108 (19) (2004) 6017–6024.
[24] J. van den Brand, S. van Gils, P.C.J. Beentjes, H. Terryn, V. Sivel, J.H.W. de Wit, Progress in Organic Coatings 51 (2004) 339.
[25] S. van Gils, C.A. Melendres, H. Terryn, Surface and Interface Analysis 35 (2003) 387.
[26] R. van Tijum, W.P. Vellinga, J.Th.M. De Hosson, Journal of Materials Science 42 (2007) 3529–3536, Workshop on Size-Dependent Effects in Materials for Environmental Protection and Energy Application, Varna, Bulgaria, May 25–27, 2006.
[27] I. Vandendael, O. Steenhaut, A. Hubin, J. Vereecken, P. Prince, F. Reniers, T. Segato, Surface and Interface Analysis 36 (8) (2004) 1093–1097.
[28] W.P. Vellinga, R. Timmerman, R. van Tijum, J.Th.M. De Hosson, International Journal of Solids and Structures 43 (November (24)) (2006) 7371–7377.
[29] W.-P. Vellinga, A. Fedorov, J.Th.M. De Hosson, Thin Solid Films 517 (2) (2008) 841–847.
[30] W.P. Vellinga, R. Timmerman, Jeff.Th.M. van Tijum, De Hosson, Applied Physics Letters 88 (6) (2006) 061912.